Journal of Nano- and Electronic Physics
Vol. **10** No 5, 05023(4pp) (2018)

Журнал нано- та електронної фізики
Том **10** № 5, 05023(4cc) (2018)

A Simple Sonochemical Synthesis of Nanosized ZnO from Zinc Acetate and Sodium Hydroxide

M.I. Zakirov, M.P. Semen'ko, O.A. Korotchenkov

Faculty of Physics, Taras Shevchenko Kyiv National University, 01601 Kyiv, Ukraine

(Received 21 July 2018; revised manuscript received 22 October 2018; published online 29 October 2018)

An efficient sonochemical route for synthesis of nano sized zinc oxide is reported. The method employs zinc acetate and sodium hydroxide as precursors with isopropyl alcohol as a solvent. As prepared powders were characterized by XRD, SEM and FTIR. These show that the resulting powder is composed of multi-domain crystallites of ZnO wurtzite, zincite and $Zn(OH)_2$. The XRD-measured coherent domain size varies from about 20 to 30 nm, whereas SEM exhibits ≈ 200 nm crystallites. The wurtzite phase is found to dominate at sonication times smaller than ≈ 30 min. It is also found that the powders produced sonochemically exhibit smaller and narrower size-distributed particles compared to that in hydrothermally prepared powders.

Keywords: Semiconductors, Chemical synthesis, Phosphors, X-ray diffraction.

DOI: 10.21272/jnep.10(5).05023 PACS numbers: 63.20. – e, 81.20

1. INTRODUCTION

One of the promising semiconducting material, which has several unique physical and chemical properties, is zinc oxide (ZnO) [1, 2]. Thus, ZnO exhibits interesting piezoelectric behavior [3], offers numerous applications in sensor and actuator systems, photocatalysis, field-emission transistors, supercapacitors, biomedical systems, ultraviolet photodetectors and solar cells [4, 5]. In the nanosized range, these properties are even more pronounced with respect to their bulk counterpart [6].

Nanosized ZnO particles have been prepared in a great number of routes, including the oxidation process, chemical vapor deposition and pulsed-laser deposition, sol-gel synthesis and combustion, polymerization, precipitation, solvothermal and hydrothermal synthesis, RF magnetron sputtering [7], etc. However, some of these methods suffer from drawbacks due to the use of high temperatures and pressures, toxic reagents and stabilizing additives.

Recently, several new routes based on a green, fast, environment-friendly sonochemical method have been developed [8, 9]. In this case, the preparation of ZnO nanoparticles is mediated by the formation, growth and collapse of bubbles in a solvent, thus making the fabrication process to be rather complicated. As a consequence, some important process variables, such as pressure amplitude and temperature, have distinct effects on the properties of the final material, while others may have only minor effects. Thus, the nature of solvent, which affects the cavitation process, is of paramount importance. In this respect, high boiling temperature of the solvent and low gas thermal conductivity are favorable, since at this condition the cavitational collapse is most extreme [10]. Therefore, various gaseous hydrocarbons (methane, ethane, ethylene and propane) with polyatomic molecules that have high heat capacities can be thought of being advantageous [11]. In particular, 1,3-propane diol has a high boiling point (210 °C) and thus can be employed in the sonochemical synthesis of nanocrystalline ZnO using zinc acetate [$Zn(CH_3COO)_2$] and 1,3-propane diol as a solvent [12].

We have recently compared the photoluminescence spectra and surface photovoltage decays in ZnO samples, prepared by hydrothermal (HT) and sonochemical (SC) methods, elucidating different formation mechanisms and resulting concentration of point defects in the HT and SC samples [13].

In this work, we demonstrate the feasibility of an extremely simple sonochemical route in obtaining ZnO nanoparticles using zinc acetate and sodium hydroxide as precursors with isopropyl alcohol (IPA, C_3H_8O, boiling point is about 82 °C) as a solvent. To our knowledge, this is the first report on the suitability of pure isopropyl alcohol for the preparation of nanosized ZnO in the sonochemical reaction without addition of surfactants.

2. EXPERIMENTAL

For synthesis, we used isopropyl alcohol (99.99 %), zinc acetate and sodium hydroxide, which were reagent grade with purity better than 99 %. All solutions were prepared with isopropyl alcohol. At first, the solutions of 1mM of zinc acetate and 0.02 M of sodium hydroxide were prepared in isopropanol and then both solutions were stepwise cooled down to 0 °C, mixed and stirred.

We carried out parallel runs for synthesis of nanosize ZnO in the presence and absence of sonication. Therefore, a part of the solution was placed in a water bath kept at 65 °C and stirred for 120 min, yielding the hydrothermally produced sample marked HT120. Another part of the solution was pre-heated to 30 °C and then placed in a home-built sonication system with a Langevin transducer, designed to work at the resonant frequency of about 30 kHz. The solution was sonicated for different sonication times, ranging from 1 to 120 min, thus producing the samples marked SC1 to SC120, respectively. The frequency was slightly tuned around ≈ 30 kHz to give cavitation bubbles in the solution.

Taking into account the general synthesis route of ZnO given, e.g., by Zak et al [9], the plausible pathway for product formation is assumed to be in a series of reactions that may be represented as follows:

$$C_3H_8O+(CH_3COO)_2Zn \rightarrow Zn^{2+}+2CH_3COO+C_3H_8O \quad (1)$$

$$NaOH \rightarrow Na^{+}+OH^{-} \quad (2)$$

$$IPA+ZnAc_{solution}+SodiumHydrox_{solution} \xrightarrow{)))} \xrightarrow{)))} ZnO/Zn(OH)_n \quad (3)$$

$$Zn^{2+}+2OH^- \xrightarrow{)))} ZnO+H_2O$$
$$Zn^{2+}+2OH^- \xrightarrow{)))} Zn(OH)_2 \xleftrightarrow{)))} ZnO+H_2O \quad (4.1\text{-}4.3)$$
$$Zn^{2+}+4OH^- \xrightarrow{)))} Zn(OH)_4^{2-} \xleftrightarrow{)))} ZnO+H_2O+2OH^-$$

where the symbol))) denotes sonication, $ZnAc_{solution}$ - zinc precursor solution. On the step 3 zinc acetate and sodium hydroxide solutions were mixed with isopropyl alcohol and started sonication. Under sonication zinc oxide and zinc hydroxide formed. Both $Zn(OH)_2$ and $Zn(OH)_4^{2-}$ act as intermediate metastable phases, which were tested, together with the resulting ZnO powder, by x-ray diffraction (XRD). We did not use centrifugation to separate the phases, which allows estimating the relative ZnO yield in the reacting solution. The thermal treatment (HT route) and sonication (SC route) resulted in white cloudy solutions, which were washed twice in distilled water and methanol, and then dried in ambient air for 12 hours at ≈ 60 °C.

As the phase separation was not made, we expect from the above reaction series that the resulting powder would consist of different phases of zinc oxide and zinc hydroxide. It is furthermore anticipated that the ratio of oxide and hydroxide phase would increase upon increasing the synthesis time. Finally, the hydroxide crystallite size is expected to be smaller than that of oxide since the former phase is metastable, which is finally transformed into the ZnO phase at prolonged sonication times.

The occurrence of zinc hydroxide metastable phases in the ambient (1 bar, 30 °C) to supercritical (300 bars, 400 °C) conditions has previously been reported [14] and the mechanism behind the phase transformation has been addressed [15]. Following the data of Ref. [14], the enthalpy change for the transformation of zinc hydroxide into zinc oxide is $\Delta H = 4.07$ kJ mol^{-1} (5.62 kJ mol^{-1} for ε-$Zn(OH)_2$) and that for transforming tetra hydroxide into oxide is $\Delta H = 0.67$ kJ mol^{-1}. It has also been observed that the hydroxide phase gives a dominant contribution at low temperatures. Therefore, it can be expected that the SC grown ZnO would arise due to (1) merging of zinc with hydroxide and (2) zinc hydroxide decomposition. In the case of HT synthesis, ZnO grows (1) by merging Zn and OH^- and also (2) by growing of zinc hydroxide.

It is therefore anticipated that the sonochemical route will produce larger zinc oxide crystallite, as is indeed the case experimentally. Furthermore, according to Ref. [16], increasing the synthesis time affects the particle morphology, which was observed by taking FTIR spectra [17]. The crystal phase, particle morphology and size turn out to vary opto-electronic properties of the powders, such as photoluminescence spectra and surface photovoltage decays. These were analyzed elsewhere [18].

To monitor the phase purity and composition of the powders, the prepared materials were characterized by XRD using Co Kα radiation and a DRON diffractometer, equipped with a Ge monochromator in the incident beam and scintillation counter detection. The XRD patterns were scanned over the 2θ angular range from 30° to 90°. Fourier transformed-infrared (FTIR) spectra were collected using a Spectrum BX-II FTIR PerkinElmer spectrometer in the spectral range from 400 to 4000 cm^{-1}. Particle size was also determined by taking scanning electron microscopy (SEM) images recorded with a JEOL JSM 6360 LA microscope.

3. RESULTS AND DISCUSSION

The XRD patterns shown in Fig. 1 indicate the crystalline nature of the product formed sonochemically (curves 1 to 3) and hydrothermally (curve 4). The XRD results clearly show three types of characteristic diffraction peaks that are in good agreement with literature values and can be indexed as ZnO hexahonal wurtzite (JCPDS No. 36-1451), ZnO hexagonal zincite (PDF No. 01-089-7102) and $Zn(OH)_2$ (PDF No. 24-1444) phases. The peak at $2\theta = 74.43°$ can probably be associated with zinc peroxide (ZnO_2) that typically formed at high temperatures and pressures [19, 20]. Finally, the peak at $2\theta = 59.78°$ observed in SC120 (curve 3) cannot be clearly identified.

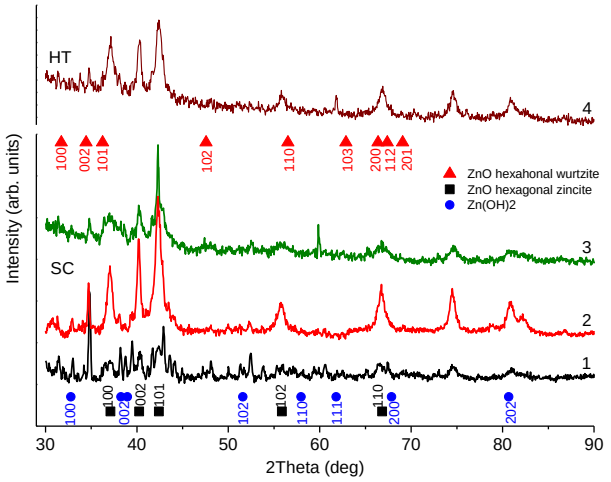

Fig. 1 – X-ray diffraction patterns of our SC (curves 1 to 3) and HT (4) samples prepared at times 30 (1), 60 (2) and 120 (3 and 4) min. Triangles mark the patterns, which are in accord with the typical (▲) hexahonal wurtzite (JCPDS No. 36-1451), (■) hexagonal zincite (PDF No. 01-089-7102) ZnO and (•) β-Zn(OH)2 (PDF No. 24-1444) diffraction

The data of Fig. 1 indicate that the XRD patterns vary in strength and width with changing the sonication time. Thus, the wurtzite phase dominate in SC30 (curve 1) whereas SC60 and SC120 samples (curves 2 and 3, respectively) are mostly composed of zincite.

A definite line broadening of the ZnO diffraction peaks clearly seen in Fig. 1 can be due to the fact that the synthesized particles are of sizes in the nanometer range. The coherent length L corresponding to the dimensions of the crystalline grains is calculated from the full width at half-maximum (FWHM) of the XRD peak β (in rad), using the Debye-Scherrer equation [21]

$$L = \frac{0.9\lambda}{\beta \cos\theta},$$

where λ is the x-ray wavelength. The crystalline sizes obtained for different planes defined by the Miller indi-

ces hkl as well as the plane-averaged size are given in Table 1.

It can be found from the XRD data that the sonochemically synthesized powders consists of a mixture of 30 % of wurtzite, 39 % of zincite and 30 % of $Zn(OH)_2$ for SC120. Appropriate values in other samples are found to be 28 %, 52 % and 18 % for SC60, and 55 %, 23 % and 21 % for SC30, respectively. Finally, the powder formed hydrothermally (HT120) is a mixture of 30 % of wurtzite, 50 % of zincite and 20 % of $Zn(OH)_2$. The phase compositions of the produced SC and HT powders are given in Fig. 2.

Table 1 -Crystallite size obtained using the Debye-Scherrer equation

Phase	ZnO (wurtzite)		ZnO (zincite)		$Zn(OH)_2$		Avarage crystalline size (nm)
Sample	hkl	Size (nm)	hkl	Size (nm)	hkl	Size (nm)	
SC30	002	43.1	101	15.2	002	37.6	32.0
SC60	002	42.6	101	16.3	202	11.5	23.5
SC120	102	44.4	101	24.5	202	18.2	29.1
HT120	200 112	11.5	101	10.3	111	49.2	19.9

SEM images of the SC120 and HT120 samples are displayed in Figs. 3a and b; histograms c and d in Fig. 3 show the size distributions of the particles, which are obtained by statistically averaging on several SEM images. The mean particle size is estimated to be (189 ± 6) and (447 ± 22) nm for the SC and HT particles, respectively. Comparison of the particle size determined from SEM to that determined from XRD (see Table 1) demonstrates that the estimated sizes appear much larger by TEM than estimated by XRD diffraction. This discrepancy can be ascribed to the fact that the XRD-measured size is attributed to coherent domains, so that the particles observed by SEM can be mostly multi-domain crystallites. Finally, the sonochemical route seems to lead to smaller particles and apparently narrower size distribution compared to that observed in samples prepared hydrothermally.

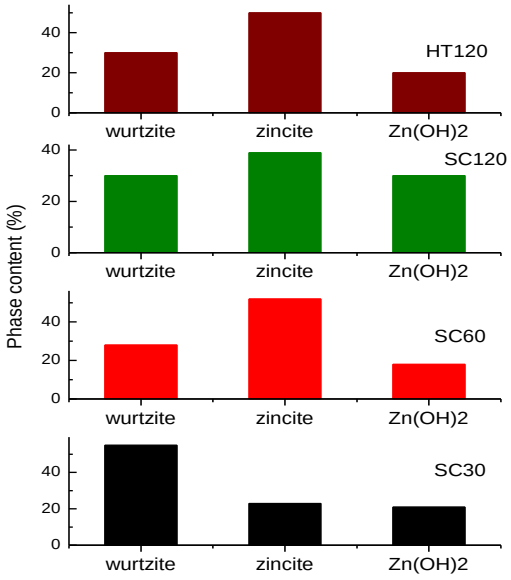

Fig. 2 – Phase composition of our SC30, SC60, SC120 and HT120 samples

The formation of ZnO particles is further supported by FTIR measurements. As shown in Fig. 4, quite similar spectra are obtained for the HT and SC samples prepared at different sonication times ranging from 1 to 120 min.

From previous studies, the absorption peak between 460 and 467 cm^{-1} is assigned to the Zn-O stretching band which is typical for ZnO wurtzite structure [4, 22]. Bulk ZnO was reported to show a broad band around 480 cm^{-1} due to the stretching mode of the zinc and oxygen bond [23]. A similar band was also observed in nano-ZnO. The Zn-O bond is also assigned to the frequency of 544 cm^{-1} for pure ZnO which is shifted to higher frequencies, up to 554 cm^{-1} in Cu doped ZnO nanopowders [22, 24]. The FTIR spectral bands at 835 and 624 cm^{-1} are also assigned to the vibrational frequencies due to the change in the microstructural features by the addition of Cu into Zn-O lattice. Incorporation of Fe in the ZnO lattice shifts the pure Zn-O bond to 680 and 836 cm^{-1} [25]. As Cu and Fe atoms are slightly lighter than Zn atom, vibrational modes in mixed Zn,Cu(Fe)O crystals exhibit an upward shift of the fundamental transverse optical phonon mode [17]. Zn-O stretching mode has also been observed in the range from 400 to 700 cm^{-1} [26, 27], particularly in the crystals with a high concentration of defects [28].

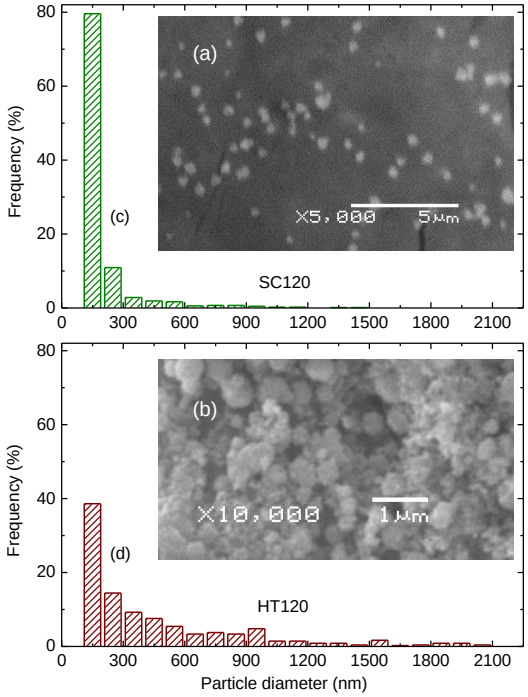

Fig. 3 – SEM images of SC120 (a) and HT120(b) samples. Histograms (c) and (d), obtained by statistically averaging over several SEM images, show the size distributions of the particles in SC120 (c) and HT120(d) samples, respectively

It is seen in Fig. 4 that vibration modes below ≈ 600 cm^{-1} are much weaker in SC samples (spectra 1 to 5) when compared to that in HT120 (spectrum 6), which can be related to better crystalline quality of the SC samples. Furthermore, the wurtzite ZnO vibration mode observed between 460 and 480 cm^{-1} is not observed at extremely small sonication times (cf. spec-

trum 1 in Fig. 4), grows remarkably at the times of about 10 min (spectrum 2) and then quench at greater sonication times (spectra 3 to 5). In clear accord, the wurtzite phase dominates in the SC30 powder mixture, which is obviously not the case in SC60, SC120 and HT120 (see Fig. 2).

A peak between 900 and 1000 cm^{-1} (arrow a in Fig. 4) seen in all spectra can be associated with Zn-OH vibrations, while two principal absorption peaks observed between 1650 and 1400 cm^{-1} (arrows b and b' in Fig. 4) correspond to the asymmetric and symmetric stretching of the carboxyl group (C=O) [29]. The broad absorption peaks ranging from about 3400 to 3500 cm^{-1} (arrow c in Fig. 4) correspond to hydrogen stretching frequency (OH– ions stretching), being related to water absorbed on the particle surfaces [29].

Nano sized ZnO can be obtained sonochemically using zinc acetate and sodium hydroxide as precursors with isopropyl alcohol. This yields a mixture of well-characterized crystalline ZnO wurtzite, zincite and $Zn(OH)_2$ in the as prepared powder, as confirmed by XRD and FTIR observations. The wurtzite phase dominates at sonication times smaller than ≈ 30 min. The sonochemical route produces smaller particles and narrower size distributions in comparison with hydrothermal synthesis.

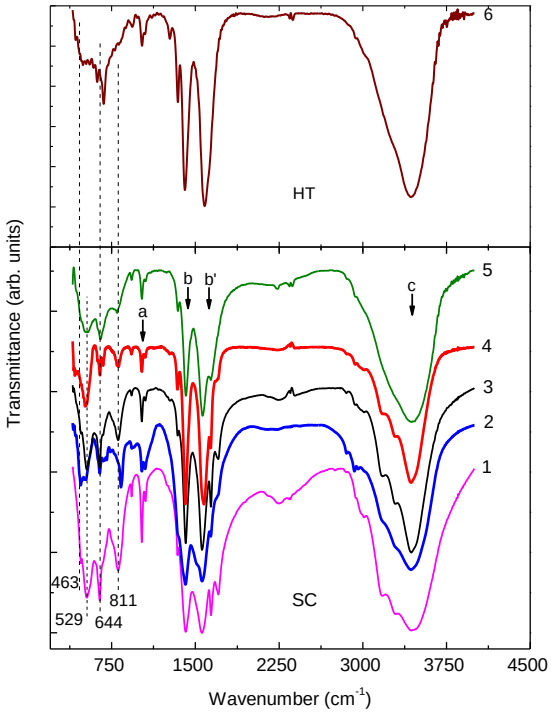

Fig. 4 – FTIR spectra of our SC (curves 1 to 5) and HT (6) samples prepared at times 1 (1), 10 (2), 30 (3), 60 (4) and 120 (5 and 6) min

REFERENCES

1. X. Fang, T. Zhai, U.K. Gautam, L. Li, L. Wu, Y. Bando, D. Golberg, *Prog. Mater. Sci.* **56**, 175 (2011).
2. R. Marczak, D. Segets, M. Voigt, W. Peukert, *Adv. Powder Technol.* **21**, 41 (2010).
3. A.V. Desai M.A. Haque, *Sensor. Actuat. A Phys.* **134**, 169 (2007).
4. X. Wu, K. Li, H. Wang, *J. Hazard. Mater.* **174**, 573 (2010).
5. A. Yildiz, S. Uzun, N. Serin, T. Serin, *Scripta Mater.* **113**, 23 (2016).
6. M. Law, J. Goldberger, P. Yang, *Annu. Rev. Mater. Res.* **34**, 83 (2004).
7. Y. Zhang, M.K. Ram, E.K. Stefanakos, D. Y. Goswami, *J. Nanomater.* **2012**, ID 624520 (2012).
8. A. Khorsand Zak, W.H.abd. Majid, H.Z. Wang, R. Yousefi, A. Moradi Golsheikh, Z. F. Ren, *Ultrason. Sonochem.* **20**, 395 (2013).
9. P. Banerjee, S. Chakrabarti, S. Maitra, B.K. Dutta, *Ultrason. Sonochem.* **19**, 85 (2012).
10. K.S. Suslick, S.-B. Choe, A.A. Cichowlas, M.W. Grinstaff, *Nature* **353**, 414 (1991).
11. W.B. McNamara, Y.T. Didenko, K.S. Suslick, *Nature* **401**, 772 (1999).
12. K.D. Bhatte, D.N. Sawant, D.V Pinjari, A.B. Pandit, B.M. Bhanage, *Mater. Lett.* **77**, 93 (2012).
13. M.I. Zakirov, V.V Kuryliuk, O.A. Korotchenkov, *J. Phys. Conf. Ser.* **741**, 012028 (2016).
14. F. Demoisson, R. Piolet, F. Bernard, *Cryst. Growth Des.* **14**, 5388 (2014).
15. M. Wang, Y. Zhou, Y. Zhang, S.H. Hahn, E.J. Kim, Y. Song, H. Chen, H. Chen, Z. Chen, *CrystEngComm* **13**, 6024 (2011).
16. P. Hayati, A.R. Rezvani, A. Morsali, D.R. Molina, S. Geravand, S. Suarez-Garcia, M.A.M. Villaecija, S. García-Granda, R. Mendoza-Meroño, P. Retailleau, *Ultrason. Sonochem.* **37**, 382 (2017).
17. K. Sowri Babu, A.R. Reddy, C. Sujatha, K.V. Reddy, A.N. Mallika, *J. Adv. Ceram.* **2**, 260 (2013).
18. M.I. Zakirov, O.A. Korotchenkov, *Mater. Sci. Pol.* **35**, 211 (2017).
19. S. Verma, S.L. Jain, *Inorg. Chem. Front.* **1**, 534 (2014).
20. W. Chen, Y.H. Lu, M. Wang, L. Kroner, H. Paul, H.-J. Fecht, J. Bednarcik, K. Stahl, Z.L. Zhang, U. Wiedwald, U. Kaiser, P. Ziemann, T. Kikegawa, C.D. Wu, J.Z. Jiang, *J. Phys. Chem. C* **113**, 1320 (2009).
21. B.D. Cullity, S.R. Stock, *Elements of X-Ray Diffraction* (Prentice Hall, 2001).
22. S. Muthukumaran, R. Gopalakrishnan, *Opt. Mater. (Amst).* **34**, 1946 (2012).
23. N. Vigneshwaran, S. Kumar, A.A. Kathe, P.V Varadarajan, V. Prasad, *Nanotechnology* **17**, 5087 (2006).
24. S. Singhal, J. Kaur, T. Namgyal, R. Sharma, *Phys. B Condens. Mat.* **407**, 1223 (2012).
25. K. Raja, P.S. Ramesh, D. Geetha, *Spectrochim. Acta Part A Mol. Biomol. Spectrosc.* **131**, 183 (2014).
26. N.F. Djaja, D.A. Montja, R. Saleh, *Adv. Mater. Phys. Chem.* **03**, 33 (2013).
27. R. Saleh, N.F. Djaja, Spectrochim, *Acta Part A Mol. Biomol. Spectrosc.* **130**, 581 (2014).
28. Z. Sharifalhoseini, M.H. Entezari, R. Jalal, *Ultrason. Sonochem.* **27**, 466 (2015).
29. A. Jain, S. Panwar, T.W. Kang, H.C. Jeon, S. Kumar, R.K. Choubey, *J. Mater. Sci. Mater. Electron.* **25**, 1716 (2014).